Symmetry-changing commensurate-incommensurate solid transition in the ^{4}He monolayer on 6,6,12-graphyne

Jeonghwan Ahn, Mujin You, Gwangyoung Lee, Tyler Volkoff, and Yongkyung Kwon[*]
Department of Physics, Konkuk University, Seoul 05029, Korea

Path-integral Monte Carlo calculations have been carried out to investigate physical properties of a ^{4}He monolayer adsorbed on a single 6,6,12-graphyne sheet, which is one of the graphyne families possessing a rectangular symmetry. To characterize elusive quantum phases of an adsorbed ^{4}He monolayer on 6,6,12-graphyne, we model the ^{4}He-graphyne interaction by the pairwise sum of empirical ^{4}He-C interatomic potentials. At partially filled ^{4}He coverages, we identify three commensurate solids of the $C_{3/4}$, $C_{4/4}$, and $C_{6/4}$ structures from the two-dimensional density distribution. These solids show the rectangular symmetry inherited from the symmetry of 6,6,12-graphyne, which were confirmed with the analysis of their static structure factors. At high helium coverages near its completion, the ^{4}He monolayer is predicted to exhibit a transition from a rectangular commensurate structure to a triangular incommensurate structure, after going through inhomogeneous structures mixed with domains of triangular and rectangular orderings. This symmetry-changing transition has not been observed in ^{4}He monolayers adsorbed on other carbon substrates.

I. INTRODUCTION

A system of ^{4}He atoms adsorbed on planar carbon and carbon-based substrates like graphite provides a model platform for the physics of low-dimensional degenerate quantum liquids. The rich quantum phase diagrams of these systems arise due to the interplay of ^{4}He-^{4}He interaction, the attractive interaction of ^{4}He atoms with the carbon lattice, and the lattice symmetry. In particular, the strong ^{4}He-substrate interaction allows helium atoms to develop multiple distinct adlayers with each layer exhibiting several phases as a function of a filling fraction [1]. For instance, a ^{4}He monolayer adsorbed on the graphite surface exhibits commensurate phases at 1/3 and 7/16 fillings, respectively, relative to the adsorption sites on the substrate and a commensurate-incommensurate (C-IC) solid transition near its completion density [2,3]. While no superfluidity has been observed in the first layer of ^{4}He atoms on graphite because of strong binding to the graphite surface, superfluid response has been observed in the second ^{4}He layer through torsional oscillator experiments [4]. This, along with the observation of anomalous melting peaks in heat capacity measurement [5], led to an early speculation of two-dimensional (2D) supersolidity. While path-integral Monte Carlo (PIMC) calculations showed no evidence of supersolidity in the second ^{4}He layer on graphite [3,6], some exotic phases, including quantum liquid crystal [7] and the coexistence of density wave order and superfluidity [8], were claimed in recent experimental studies for this 2D ^{4}He system.

Recently, quantum phase diagrams of ^{4}He adlayers on other 2D carbon substrates have been pursued in a similar context to the above studies. On a single graphene sheet,

incommensurate and commensurate solids (first layer) and quantum liquid (second layer) phases analogous to those on graphite were observed in the adsorbed ^{4}He layers [9–11] despite weaker attractive interactions. On the other hand, on graphynes [12–14], which are newly proposed 2D carbon allotropes consisting of sp- and sp^2-bonded carbon atoms (Fig. 1), ^{4}He adatoms reveal somewhat more complex and various quantum phases compared to graphene, due to a variety of combinations of benzene ring and acetylene chain substructures.

For instance, a transition between a Mott insulating phase and commensurate solid phase was observed in the ^{4}He monolayer above the α-graphyne surface. This can be understood in terms of symmetry-breaking process of an arrangement of Ising pseudospin degrees of freedom which corresponds to two isoenergetic configurations for three ^{4}He atoms in the hexagon cell [15]. In addition, the presence of a corresponding layer adsorbed on the opposite side of a single sheet of α-graphyne induces helium atoms in a given hexagon to align in parallel or antiparallel to the pseudospin in the corresponding hexagon of the opposite layer. These alignments can be explained by interlayer correlation of the ^{4}He monolayers across the substrate [16]. Furthermore, the first adsorbed ^{4}He monolayer on γ-graphyne exhibits three different commensurate solid phases, followed by the C-IC transition at higher densities [17].

In this paper we investigate the quantum phase diagram of the first ^{4}He layer adsorbed on a single sheet of 6,6,12-graphyne by using PIMC method. Unlike α- and γ-graphyne, 6,6,12-graphyne has a rectangular symmetry [Fig. 1(c)] which supports various adsorbed commensurate solids with the same rectangular symmetry. In addition to rectangular commensurate solids, high-density triangular incommensurate solids can be expected in the first ^{4}He layer. We show that the
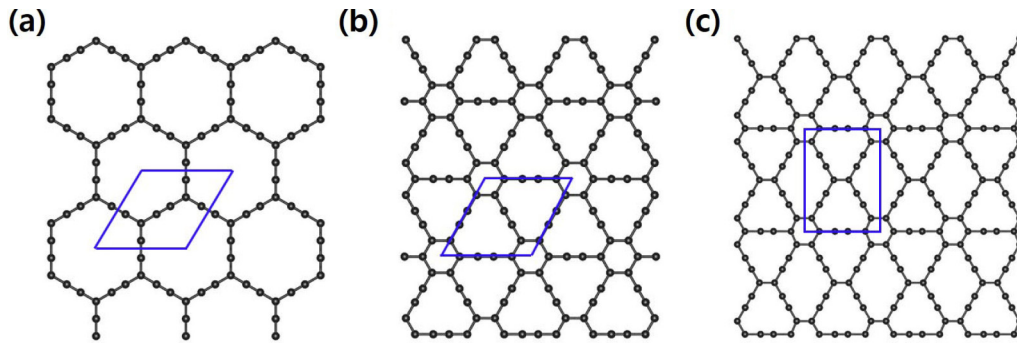
*ykwon@konkuk.ac.kr

FIG. 1. Structures of (a) α-graphyne, (b) γ-graphyne, and (c) 6,6,12-graphyne. The blue parallelograms represent the primitive cells of the respective graphyne structures.

first ^{4}He layer on 6,6,12-graphyne exhibits three different commensurate solids with rectangular symmetry. A promotion to the second adsorbed layer begins at densities greater than the densest commensurate solid phase ($C_{6/4}$). Near the completion density, corresponding to saturation of the first layer, the rectangular helium solid gives way to a triangular incommensurate solid, from which we infer that substrate symmetry plays a role in determining quantum phases of the first ^{4}He layer. Unlike the C-IC transition observed in ^{4}He on graphite [2,3] or on γ-graphyne [17], the present C-IC phase transition involves a symmetry change, which has not been observed in previously investigated ^{4}He adlayers on any carbon substrates.

II. METHODOLOGY

In our study, all carbon atoms are fixed at the lattice points of 6,6,12-graphyne while quantum dynamics of ^{4}He atoms, along with their quantum statistics, are fully incorporated with the path integral formalism. We use a conventional PIMC algorithm proposed by Ceperley [18]. The ^{4}He-graphyne interaction is described by a sum of pair interactions between a ^{4}He atom and carbon atoms in the 6,6,12-graphyne surface located at $z = 0$.

To describe the ^{4}He-C pair interaction we use an isotropic 6-12 Lennard-Jones potential proposed to fit scattering data of helium atoms from graphite surfaces [19,20]. For the ^{4}He-^{4}He pair interaction, we use the well-known Aziz potential obtained by the Hartree-Fock dispersion potential energy models [21]. In our discrete path integral representation, the thermal density matrix at a low temperature T is factored into M high temperature density matrices with an imaginary time step $\tau = (Mk_BT)^{-1}$.

The ^{4}He-C pair potential and the ^{4}He-^{4}He potential are incorporated with exact two-body density matrices at the high temperature MT [18,22]. In this treatment, a time step $\tau^{-1}/k_B = 40$ K is found to be short enough to provide an accurate description for the ^{4}He-graphyne interaction as well as the ^{4}He-^{4}He interaction [23]. The same time step was also used in our previous PIMC studies for the ^{4}He-graphyne systems [16,17]. Noting that our ^{4}He-graphyne potential is described by using the parameters derived for an interatomic potential between a ^{4}He atom and an sp^2-bonded carbon atom of graphite, we tested the robustness of our modeling of the ^{4}He-graphyne potential by varying the ^{4}He-C pair potential

used. Changing the well depth of the interatomic potential between a ^{4}He atom and an sp-bonded carbon atom in graphyne by $\pm15\%$ resulted in little difference in the structural properties of the system [23]. From this we conclude that the quantum phase diagram presented in Fig. 6 (see below) is valid even though our ^{4}He-graphyne potential is based on empirical ^{4}He-C pair potentials derived to describe the ^{4}He-graphite interaction.

The periodic boundary conditions are applied to a 4×3 rectangular simulation cell with the size of 27.44×28.38 Å^2 along the xy plane to overcome finite sizes of our planar system, and no boundary condition is imposed for the vertical direction to the graphyne surface.

III. RESULTS

A. One-dimensional density distributions

We first observe layer-by-layer development of ^{4}He adatoms above the single sheet of 6,6,12-graphyne by computing one-dimensional (1D) density distributions along the vertical direction to the graphyne surface (see Fig. 2). The
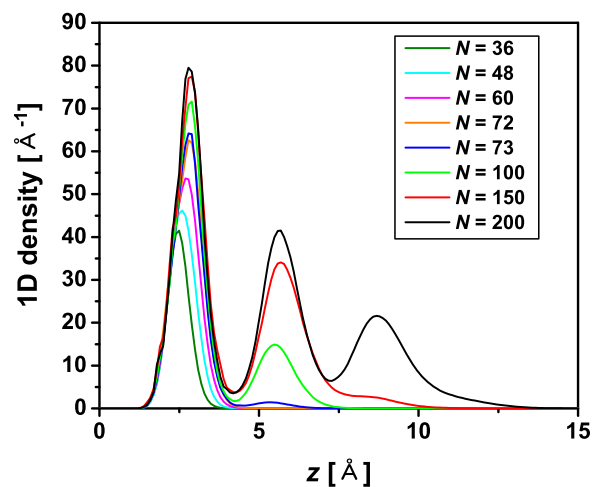

FIG. 2. One-dimensional density distributions for ^{4}He atoms adsorbed on a single 6,6,12-graphyne sheet as a function of the vertical distance z from the graphyne surface. Here N represents the number of ^{4}He atoms per 4×3 rectangular simulation cell with the size of 27.44×28.38 Å^2.

computations were done at a temperature of 0.5 K and all simulations started from ^{4}He random configurations in the half-space $z > 0$ whose initial positions are far away ($\gtrsim 8$ Å) from the graphyne surface. Unlike the case of α-graphyne [15,16], it was found that no helium atoms occupy the in-plane centers of hexagons in 6,6,12-graphyne, so that the 1D distributions shown in Fig. 2 are attributed to only ^{4}He layers adsorbed on top of the graphyne sheet. From the sharp peaks in Fig. 2, we confirm the formation of up to three distinct ^{4}He layers and their subsequent development as the particle number increases. A promotion to the second ^{4}He layer is found to start above 73 ^{4}He atoms per 4×3 simulation cell, which corresponds to the areal density of 0.0937 Å^{-2}. This value for the promotion density can be understood by the fact that 6,6,12-graphyne rectangular symmetry-induced commensurate structure formed with 72 ^{4}He atoms per simulation cell tends to be sustained under low-density compression by additional helium atoms. Further addition of helium atoms compresses the underlying solid and results in the first layer being completed at $\sim$0.113 Å^{-2}, where we observe the highest first-layer density achievable in our simulation. At the completion density, a triangular incommensurate structure is expected for an extended ^{4}He-graphyne system since the contribution of the ^{4}He-^{4}He interactions becomes more dominant in this high density regime than the ^{4}He-graphyne interaction. The estimated completion density is comparable to the corresponding values predicted for α- and γ-graphyne [15,17], which is understandable when considering similar surface densities of carbon atoms in these graphyne structures.

B. Two-dimensional density distributions

To identify structural properties of the first ^{4}He layer adsorbed on top of the graphyne substrate, the density distributions along the lateral directions are analyzed. We present in Fig. 3 the 2D density distributions of the ^{4}He monolayer at the areal densities of 0.0462, 0.0616, 0.0925, and 0.109 Å^{-2}. A distinct peak in the figure corresponds to a single occupancy of ^{4}He atom in the monolayer. In Fig. 3(a) we observe that each irregular hexagon in 6,6,12-graphyne accommodates a single helium atom at the center. This results in a commensurate solid structure characterized by a rectangular lattice with three basis atoms, whose primitive vectors are denoted by white arrows in the figure. Because there are four adsorption sites per unit cell of 6,6,12-graphyne on which three helium atoms could be bound by the substantial potential, this commensurate structure corresponds to a $C_{3/4}$ commensurate structure. In Fig. 3(b), one can see that a $C_{4/4}$ commensurate structure is formed at an areal density of 0.0616 Å^{-2} where every hexagon center of graphyne is occupied by a single ^{4}He atom. We note that the areal density of this $C_{4/4}$ structure is near the $C_{1/3}$ density on graphite. However, beyond the $C_{4/4}$ density, one expects the ^{4}He-^{4}He interaction to compete with the ^{4}He-graphyne interaction for contribution to the quantum phases of the first helium layer. As presented in Fig. 3(c), ^{4}He adatoms are crystallized into a rectangular solid at the high areal density of 0.0925 Å^{-2}, corresponding to the accommodation of six helium atoms per every four adsorption sites in each unit cell. This $C_{6/4}$ phase corresponds to the $C_{4/3}$

phase on γ-graphyne (see Fig. 4(d) of Ref. [17]) in a sense that both are high-density commensurate solids and the promotion of ^{4}He atoms to the second layer was observed beyond these commensurate densities for both cases. Considering that they have similar areal densities (0.0982 Å^{-2} for the $C_{4/3}$ phase on γ-graphyne and 0.0925 Å^{-2} for the $C_{6/4}$ phase on 6,6,12-graphyne) and γ- and 6,6,12-graphynes have similar porosities (see Fig. 1), the strength of the ^{4}He-^{4}He interaction relative to the ^{4}He-substrate interaction is similar in both phases. From this we understand that the different substrate symmetry is a main reason why one is a triangular solid (the $C_{4/3}$ phase on γ-graphyne) and the other is a rectangular solid (the $C_{6/4}$ phase on 6,6,12-graphyne). Consequently, the rectangular symmetry of 6,6,12-graphyne, in addition to the relative strength of the ^{4}He-^{4}He and the ^{4}He-graphyne interaction, plays a role in determining the quantum phases of the first ^{4}He layer on the graphyne surface at high helium coverage.

Moreover, in order to consider the effect of vacancies [24], we carried out simulations beginning from one or two fewer helium atoms over the perfect $C_{3/4}$, $C_{4/4}$, and $C_{6/4}$ commensurate solids and found that the vacancies are immobile defects in these phases. In particular, for a single vacancy (double vacancy), we find that the two-dimensional density of $N-1$ ($N-2$) particles exhibits $N-1$ ($N-2$) peaks, which coincide with their original locations in the corresponding commensurate phases. If the vacancies were mobile, one would expect to observe N density peaks with reduced amplitudes, implying the mechanism of vacancy diffusion. The immobility of vacancies is consistent with the lack of superfluidity in the first-layer commensurate solids; indeed, our PIMC calculations based on the conventional multilevel algorithm [18] showed no superfluidity in the first ^{4}He layer on 6,6,12-graphyne at 0.5 K.

Finally, additional ^{4}He adsorption on top of the $C_{6/4}$ solid induces the first ^{4}He layer to transition to an incommensurate solid regime with the first layer being compressed by the second layer. Figure 3(d) represents an incommensurate structure at the first-layer completion density of 0.113 Å^{-2}, which is seen to be mostly arranged with triangular orderings with some domains of rectangular orderings (see different domains separated by yellow dotted lines in the figure).

It is found that these triangularly ordered domains subsequently expand in larger simulation cells and a fraction of rectangular domains tends to decrease with the increase of the simulation cell size [23].

From this we predict that the first ^{4}He layer will be completed as a fully triangular incommensurate structure on the infinitely extended graphyne surface. In contrast to the C-IC transitions observed in the case of graphite [2,3] and γ-graphyne surfaces [17], the present results show that the C-IC solid transition in the first ^{4}He layer on 6,6,12-graphyne is accompanied by a symmetry change from a rectangular solid to a triangular one.

C. Energetics

The energetics of the ^{4}He system on 6,6,12-graphyne confirms the above observations from the 1D and 2D density
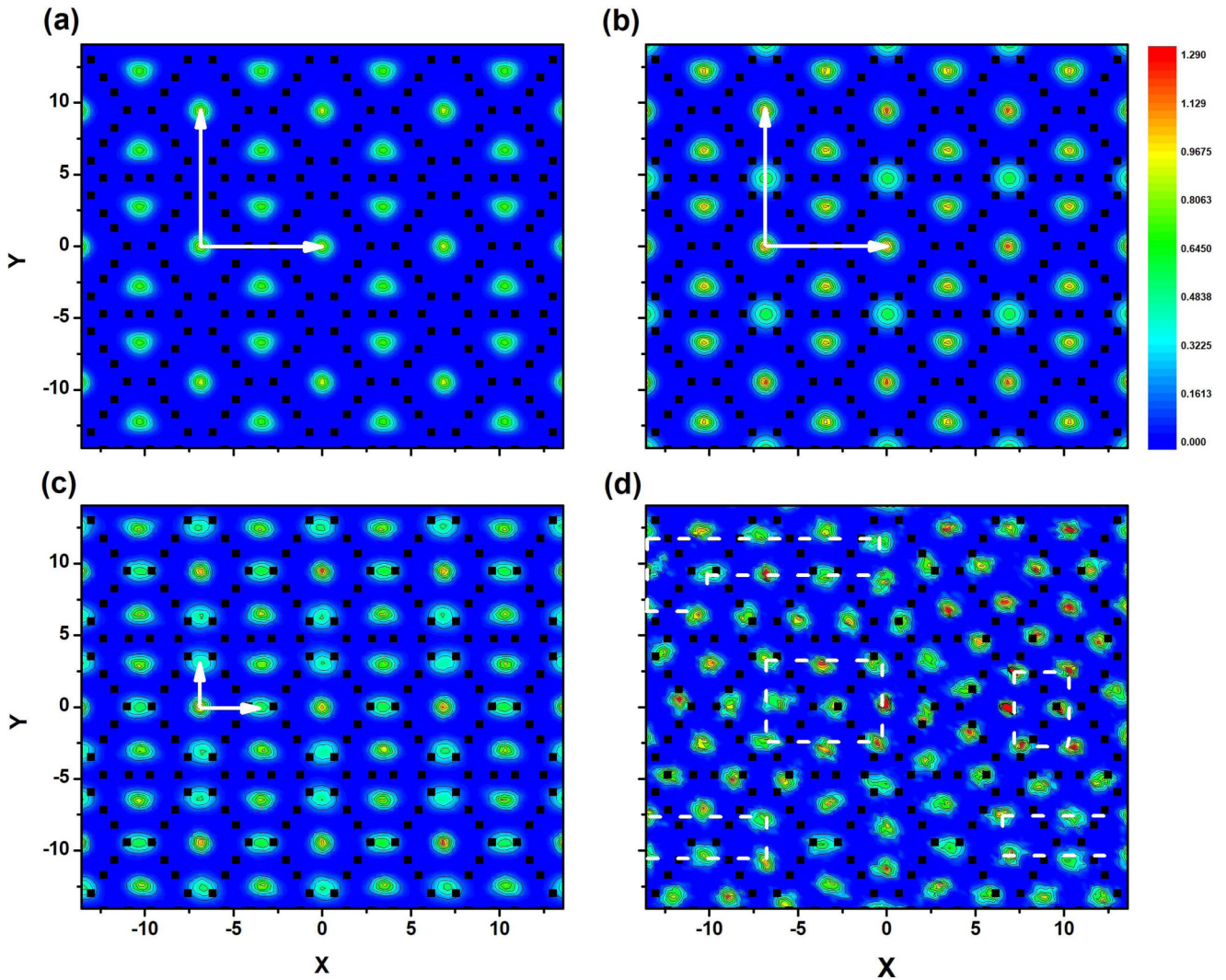
FIG. 3. Two-dimensional density distributions for the first-layer ^{4}He atoms adsorbed on the 6,6,12-graphyne surface at areal densities of (a) 0.0462, (b) 0.0616, (c) 0.0925, and (d) 0.113 Å^{-2}, which correspond to the number of the first-layer ^{4}He atoms $N = 36$, 48, 72, and 88, respectively, per 4×3 simulation cell. The black dots represent the locations of the carbon atoms in 6,6,12-graphyne. The computations were done at a temperature of 0.5 K and the length unit is Å. The white arrows in (a)–(c) represent a set of primitive lattice vectors for each solid while the white dotted lines in (d) separate two domains of triangular and rectangular orderings. All contour plots are in the same color scale denoted by the color bar on the right-hand side.

distributions. Figure 4 displays the PIMC energy per ^{4}He atom in the first layer, which was computed for the 4×3 simulation cell, as a function of areal density. At helium coverages below 0.0616 Å^2 ($C_{4/4}$ density), there is little change in the energy, indicating that effects of ^{4}He-^{4}He interaction are minimal at low helium densities. More specifically, the energy per atom decreases slightly until the energy minimum state of the $C_{3/4}$ phase is reached at 0.0462 Å^{-2}, and subsequently increases gradually up to the $C_{4/4}$ phase. This reflects the fact that a single ^{4}He atom occupies large hexagon sites (global potential minima) until the formation of the $C_{3/4}$ structure in which large hexagon sites are fully accommodated. Subsequent filling of small hexagon sites results in gradual increase of the averaged energy. Beyond the $C_{4/4}$ density at which every adsorption site is fully occupied, the energy per atom is observed to monotonically increase. This can be understood by the fact

that the system enters into a regime where some ^{4}He adatoms occupy the intermediate region between the adsorption sites and the ^{4}He-^{4}He interaction competes with the ^{4}He-graphyne interaction. We note a significant jump in the energy right after the $C_{6/4}$ commensurate density of 0.0925 Å^2, which is consistent with the observation of the promotion to the second layer for $N = 73$ in Fig. 2. In addition, we analyzed effects of the finite size of our simulation cell on the energy of the first-layer ^{4}He atoms. For three commensurate phases, the energies per atom computed for larger simulation cells were found to change very little from the values presented in Fig. 4, whose details can be seen in Fig. 3(a) of the Supplemental Material [23]. This suggests that the finite size of our simulation cell does not affect the energy per atom for the commensurate phases and hence their energetic stability.
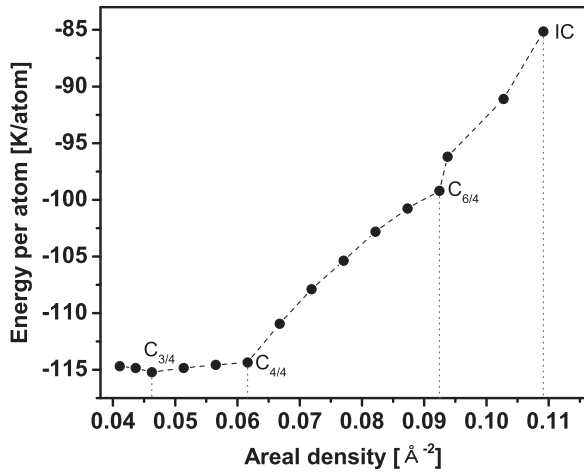
FIG. 4. PIMC energy per ^{4}He atom for the first ^{4}He layer on the 6,6,12-graphyne surface as a function of its areal density. The vertical dotted lines correspond to the areal densities for the $C_{3/4}$, $C_{4/4}$, $C_{6/4}$ phases and the incommensurate (IC) structure whose density distributions are presented in Fig. 3(d). The computations were performed at $T = 0.5$ K and statistical errors are smaller than the symbol sizes.

D. Static structure factors

The formation of different commensurate structures in a ^{4}He monolayer on 6,6,12-graphyne are further analyzed with computation of structure factor. Figure 5 presents static structure factors divided by the numbers of ^{4}He atoms for the 4×3 simulation cell, as functions of the magnitude of the wave vector, at three commensurate helium coverages. Many distinct peaks observed in the figure are due to various
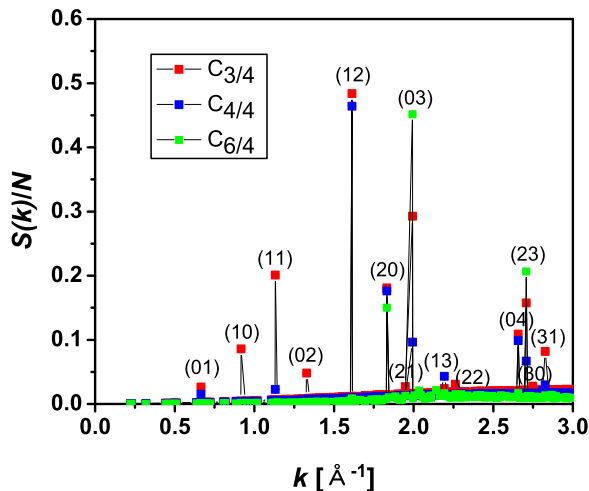

FIG. 5. Static structure factors divided by the number of ^{4}He atoms as a function of the magnitude of the wave vector k for the first ^{4}He layer on 6,6,12-graphyne. The red, blue, and green symbols represent the PIMC results for the $C_{3/4}$, $C_{4/4}$, and $C_{6/4}$ commensurate densities, respectively. The indices in parentheses represent the coordinates of the wave vector in terms of the reciprocal primitive vectors of the rectangular graphyne lattice. The computations were done at a temperature of 0.5 K with the 4×3 rectangular simulation cell. The statistical errors are smaller than the symbol sizes.

commensurate orderings of the ^{4}He adatoms that reflect the rectangular symmetry of the underlying graphyne lattice. The indices assigned to each peak in Fig. 5 represent the coordinates of the corresponding reciprocal lattice vectors.

Among the three commensurate helium coverages considered here, the number of the structure factor peaks decreases with the increase in the ^{4}He density and the $C_{3/4}$ structure displays the most structure factor peaks. For instance, the (01) peak, which corresponds to an ordering along the y axis with the periodicity of the graphyne unit cell, is observed at the $C_{3/4}$ and $C_{4/4}$ commensurate coverages. However, the peak height of the $C_{4/4}$ structure is significantly suppressed when compared to that of the $C_{3/4}$ structure, because of the presence of one more ^{4}He atom per unit cell in the former. The corresponding peak is invisible in the $C_{6/4}$ structure because of destructive interference, which can be understood by the fact that its rectangular lattice constant in the y direction is one third of the corresponding value of the underlying graphyne lattice [see Fig. 3(c)].

We note that the most strong peak appears at $k = 1.6135$ Å^{-1}, which corresponds to the (12) reciprocal lattice vector of the graphyne lattice. This (12) peak represents a diagonal ordering in the half-period graphyne unit cell along the y axis and is absent again at the $C_{6/4}$ helium coverage because of destructive interference by the intermediate helium atoms in the half-period graphyne cell. Another structure factor peak is located at $k = 1.8318$ Å^{-1} which corresponds to the magnitude of the (20) reciprocal lattice vector. This peak for the $C_{6/4}$ helium coverage results from an ordering with a half of the unit-cell length along the x axis. However, both the $C_{3/4}$ and the $C_{4/4}$ structures do not possess the periodicity of a half of the graphyne lattice parameter along the x axis but still show the sharp peaks at $k = 1.8318$ Å^{-1}. These peaks for the $C_{3/4}$ and the $C_{4/4}$ structures are originated from local hexagonal orderings of ^{4}He atoms centered at a benzene ring of graphyne. This hexagonal ordering centered at a benzene ring was also observed in a ^{4}He monolayer on γ-graphyne (see in Fig. 4(b) of Ref. [17]), where a structure factor peak was also observed at $k = 1.8318$ Å^{-1}.

In addition, the structure factor divided by the number of ^{4}He atoms at each of the three commensurate phases was found to show nearly the same peak heights for four different sizes of the 3×3, 4×3, 4×4, and 6×4 simulation cells [23]. This also confirms our conclusion that the manifestation of the aforementioned commensurate solids in the ^{4}He monolayer on 6,6,12-graphyne is not affected by the finite sizes of our simulation cells.

E. Phase diagram

Finally, we propose a phase diagram of the first ^{4}He layer adsorbed on the 6,6,12-graphyne surface as summarized in Fig. 6. According to our PIMC calculations, the first ^{4}He layer exhibits three different commensurate solid structures, i.e., $C_{3/4}$, $C_{4/4}$, and $C_{6/4}$, each having rectangular symmetry. At intermediate densities, domain-wall structures are expected with partial commensurate ordering mixed with incommensurate ordering. It is found that promotion of ^{4}He atoms to the second helium layer occurs at densities just beyond the $C_{6/4}$
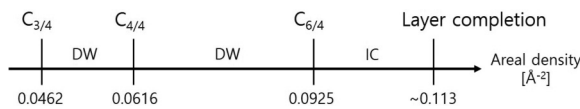
FIG. 6. Schematic phase diagram of the first ^{4}He layer adsorbed on the 6,6,12-graphyne surface as a function of an areal density.

phase where the first ^{4}He layer enters into an incommensurate solid regime under compression by the promoted atoms. We identify that the first helium layer is completed at $\sim 0.113\,\text{Å}^{-2}$ to become a triangular incommensurate solid.

IV. CONCLUSION

We have performed PIMC calculations to investigate the quantum phases of the first ^{4}He layer adsorbed on 6,6,12-graphyne. Unlike the case of ^{4}He adsorbed on graphite (graphene) [2,3] or other graphyne substrates [16,17], the helium adatoms in the first ^{4}He layer on 6,6,12-graphyne exhibit a C-IC solid transition characterized by a rectangular-to-triangular symmetry change. This suggests that the substrate symmetry, in addition to the competition between the ^{4}He-^{4}He interaction and the ^{4}He-substrate interaction strength, plays a role in determining quantum phase of the first-layer ^{4}He atoms at high helium coverages. Before crystallizing into an incommensurate solid near its completion, the first ^{4}He layer exhibits three rectangularly symmetric commensurate structures of $C_{3/4}$, $C_{4/4}$, and $C_{6/4}$ phases at intermediate ^{4}He densities. This rich set of quantum phases observed in

the ^{4}He monolayer on 6,6,12-graphyne is due to large hexagon area as well as its more porous nature than graphite or graphene. A route for future studies is provided by the fact that the ^{3}He-C pair potential as well as ^{3}He-^{3}He interaction is similar to the corresponding interaction for ^{4}He atoms, so that one can consider quantum phase diagram of adsorbed ^{3}He instead of ^{4}He on 6,6,12-graphyne in the light of some theoretical studies for ^{3}He on graphite by means of fixed-node diffusion Monte Carlo method [25–28] to deal with a fermionic sign problem effectively. These adsorbed fermionic systems could comprise various geometries of nuclear spin arrays, depending on the symmetry of ^{3}He solids, so that they can serve as a testbed to examine some spin models in the ^{3}He solids. Unlike the corresponding system on graphite [29,30], we can expect a realization of an antiferromagnetism in this spin system without geometrical frustration under its rectangular symmetry. Possible interlayer correlation between ^{4}He monolayers adsorbed on the opposite sides of a 6,6,12-graphyne sheet is currently under investigation.

ACKNOWLEDGMENTS

[1] G. Zimmerli, G. Mistura, and M. H. W. Chan, Phys. Rev. Lett. **68**, 60 (1992).

[2] D. S. Greywall and P. A. Busch, Phys. Rev. Lett. **67**, 3535 (1991).

[3] P. Corboz, M. Boninsegni, L. Pollet, and M. Troyer, Phys. Rev. B **78**, 245414 (2008).

[4] P. A. Crowell and J. D. Reppy, Phys. Rev. B **53**, 2701 (1996).

[5] D. S. Greywall, Phys. Rev. B **47**, 309 (1993).

[6] J. Ahn, H. Lee, and Y. Kwon, Phys. Rev. B **93**, 064511 (2016).

[7] S. Nakamura, K. Matsui, T. Matsui, and H. Fukuyama, Phys. Rev. B **94**, 180501(R) (2016).

[8] J. Nyéki, A. Phillis, A. Ho, D. Lee, P. Coleman, J. Parpia, B. Cowan, and J. Saunders, Nat. Phys. **13**, 455 (2017).

[9] M. C. Gordillo and J. Boronat, Phys. Rev. Lett. **102**, 085303 (2009).

[10] Y. Kwon and D. M. Ceperley, Phys. Rev. B **85**, 224501 (2012).

[11] J. Happacher, P. Corboz, M. Boninsegni, and L. Pollet, Phys. Rev. B **87**, 094514 (2013).

[12] R. H. Baughman, H. Eckhardt, and M. Kertesz, J. Chem. Phys. **87**, 6687 (1987).

[13] V. R. Coluci, S. F. Braga, S. B. Legoas, D. S. Galvão, and R. H. Baughman, Nanotechnology **15**, S142 (2004).

[14] D. Malko, C. Neiss, F. Viñes, and A. Görling, Phys. Rev. Lett. **108**, 086804 (2012).

[15] Y. Kwon, H. Shin, and H. Lee, Phys. Rev. B **88**, 201403(R) (2013).

[16] J. Ahn, S. Park, H. Lee, and Y. Kwon, Phys. Rev. B **92**, 035402 (2015).

[17] J. Ahn, H. Lee, and Y. Kwon, Phys. Rev. B **90**, 075433 (2014).

[18] D. M. Ceperley, Rev. Mod. Phys. **67**, 279 (1995).

[19] W. E. Carlos and M. W. Cole, Surf. Sci. **91**, 339 (1980).

[20] M. W. Cole and J. R. Klein, Surf. Sci. **124**, 547 (1983).

[21] R. A. Aziz, M. J. Slaman, A. Koide, A. R. Allnatt, and W. J. Meath, Mol. Phys. **77**, 321 (1992).

[22] R. E. Zillich, F. Paesani, Y. Kwon, and K. B. Whaley, J. Chem. Phys. **123**, 114301 (2005).

[23] See Supplemental Material at http://link.aps.org/supplemental/10.1103/PhysRevB.99.024113 for details of time step errors, a validity test of our ^{4}He-graphyne potential, finite size analysis, and high-density incommensurate structures.

[24] A. F. Andreev and I. M. Lifshitz, Zh. Eksp. Teor. Fiz. **56**, 2057 (1969) [Sov. Phys. JETP **29**, 1107 (1969)].

[25] M. C. Gordillo and J. Boronat, Phys. Rev. B **94**, 165421 (2016).

[26] M. C. Gordillo and J. Boronat, Phys. Rev. Lett. **116**, 145301 (2016).

[27] M. Ruggeri, E. Vitali, D. E. Galli, M. Boninsegni, and S. Moroni, Phys. Rev. B **93**, 104102 (2016).

[28] M. C. Gordillo and J. Boronat, Phys. Rev. B **97**, 201410 (2018).

[29] R. Masutomi, Y. Karaki, and H. Ishimoto, Phys. Rev. Lett. **92**, 025301 (2004).

[30] H. Fukuyama, J. Phys. Soc. Jpn. **77**, 111013 (2008).